Positive, negative, zero refraction, and beam splitting in a solid/air phononic crystal: Theoretical and experimental study

J. Bucay,[1] E. Roussel,[2] J. O. Vasseur,[2] P. A. Deymier,[1] A-C. Hladky-Hennion,[2] Y. Pennec,[2] K. Muralidharan,[1] B. Djafari-Rouhani,[2] and B. Dubus[2]

[1]*Department of Materials Science and Engineering, University of Arizona, Tucson, Arizona 85721, USA*

[2]*Institut d'Electronique, de Micro-électronique et de Nanotechnologie, UMR CNRS 8520, Cité Scientifique, 59652 Villeneuve d'Ascq Cedex, France*

(Received 15 January 2009; revised manuscript received 7 April 2009; published 25 June 2009)

We report on a phononic crystal (PC) consisting of a square array of cylindrical polyvinylchloride inclusions in air that exhibits positive, negative, or zero refraction depending on the angle of the incident sound beam. For all three cases of refraction, the transmitted beam undergoes splitting upon exiting the crystal. These properties are analyzed theoretically using finite difference time domain method and are demonstrated experimentally. Band structures and equifrequency surfaces (EFSs) calculated with the plane-wave expansion method show that the observed properties result from the unique geometry of the PC's EFS as compared to that of the incident media.

DOI: 10.1103/PhysRevB.79.214305 PACS number(s): 63.20.−e, 43.20.+g, 43.40.+s

I. INTRODUCTION

Phononic crystals (PCs) have been the subject of much study over the past few decades because of their ability to exhibit a multitude of different properties. Phononic crystals are the acoustic counterparts to photonic crystals, consisting of periodic arrangements of inclusions in a physically dissimilar matrix. The periodicity as well as the differences in the impedance of the constituent materials can cause Bragg scattering, leading to selectivity in which at certain frequencies wave propagation is forbidden. This has led to the development of PCs which exhibit complete band gaps and wave guiding properties.[1–12] More recently, research in the field has shifted to studying structures which exhibit negative and zero-angle refraction. PCs exhibiting a negative-refractive index have been developed for novel focusing devices.[13–16] Materials exhibiting zero refraction have also garnered attention because of their potential use as collimators. Wave collimation occurs when Bloch modes are excited on flat portions of a PC's equifrequency surface (EFS).[17–22] Most work in phononics and photonics which concerns collimation often employs a crystal arranged in a square lattice to produce the appropriate square EFSs.[17–20,23–25] The use of EFSs in an extended zone scheme allows one to see all of the possibly excited Bloch modes within the crystal. This scheme has also provided a means of explaining observed beam splitting in certain systems,[26–28] which can be attributed to multiple Bloch modes satisfying phase-matching conditions and leading to higher orders of refraction. The demonstration of a system which exhibits all of these characteristics (positive, negative, and zero refraction, as well as beam splitting) is highly dependent on various features of the corresponding equifrequency surfaces (EFSs) of the crystal. As such, in this paper we present a PC consisting of a square array of cylindrical polyvinylchloride (PVC) inclusions in air. This system had been studied previously for its ability to exhibit a large band gap in the audible range of frequencies. By removing a row of inclusions, frequencies within the stop band were allowed to be transmitted, demonstrating the structure's ability to be used as a frequency filter.[29] At the time of this study, most of the work in phononics was concerned with the use of PCs as acoustic filters and insulators,[29–32] as a result, little about this system's refractive behavior or beam splitting ability was explored. Through further investigation, we have found that the PC can produce positive, negative, or zero refraction depending on the angle of incidence. For all three cases, the transmitted beam undergoes splitting upon exiting the crystal. In our analysis, these properties are demonstrated theoretically using a finite difference time domain (FDTD) method, as well as experimentally. We also use the plane-wave expansion (PWE) method to calculate the band structure and EFSs for the PC. We show, by the geometry of the EFSs compared to that of the incident medium, the mechanism from which we obtain different types of wave refraction and subsequent beam splitting upon exit of the crystal.

This paper is organized as follows. In Sec. II we describe the experimental setup and theoretical models used to study the PVC/air phononic crystal. Theoretical and experimental results are reported and discussed in Sec. III. Finally, the conclusions drawn from this study are presented in Sec. IV.

II. MODEL AND METHODS

We experimentally and theoretically explore wave propagation through a PC consisting of a square array of cylindrical PVC inclusions in air. The radius of the inclusions is $r=12.9$ mm and the lattice parameter of the array is $a=27$ mm. The PWE (Ref. 3) method was employed to calculate the band structure and EFSs of the system. This method has been widely used in both the fields of phononics and photonics for its ability to reduce solving the governing equations to an eigenvalue problem by the Fourier expansion of the elastic displacement (or electromagnetic) field and of the physical parameters of the constituent materials along reciprocal-lattice vectors. The PWE calculations were performed by considering the PVC inclusions as infinitely rigid[3] and of infinite length along the z direction. 441 reciprocal

space vectors were taken into account to ensure convergence. FDTD simulations were employed to shed light on the propagation behavior through the crystal and also upon the exit. This method is based on a discretization of the equations of propagation of elastic waves in an inhomogeneous media. We take the z direction of our system to be much larger than the other spatial dimensions, which allows us to treat the system as two dimensional. As such, the governing equations take the following form:

$$\frac{\partial^2 u_i}{\partial t^2} = \frac{1}{\rho}\frac{\partial T_{ij}}{\partial x_j}, \tag{1}$$

$$T_{ij} = C_{ijkl} e_{kl}, \tag{2}$$

$$e_{ij} = \frac{1}{2}\left(\frac{\partial u_i}{\partial x_j} + \frac{\partial u_j}{\partial x_i}\right), \tag{3}$$

where u_i is the ith component of the total displacement vector, T_{ij} are the elements of the entire stress tensor, e_{kl} are the strain components, and C_{ijkl} and ρ_i are the elastic constants and density of the material, respectively. Discretization of these equations is performed in the time and space domains on a square grid. This method has been proven to be an efficient tool for the study of wave propagation in PCs.[8,30–32] For a more detailed description of this method we refer the reader to Sigalas *et al.*[33] where the fully discretized equations are presented. Because analysis of this system includes comparisons between results obtained with the FDTD as well as the PWE methods, it was necessary to use an interval of a/70 for the discretization of space and 2^{17} time steps, where $dt = 2.64 \times 10^{-8}$ sec, to ensure a convergence of results between the two methods. Both of these values satisfy the Courant condition and lead to a stable algorithm. Mur boundary conditions were imposed on all four sides of the simulation cell to avoid reflections.[34]

For the analysis of wave propagation through the PVC/air PC, two types of sources were modeled. For simulations exploring the relationship between the sign of the index of refraction of the PC for different angles of incidence, a plane-wave source (namely, source 1) was modeled using a slanted line of grid points corresponding to the desired angle in incidence of the emitted wave. Vertical and horizontal components of the source's displacement were weighted by a factor of $\cos(\theta)$ and $\sin(\theta)$, respectively, so that the sum of the two components resulted in wave propagation in a single direction of θ degrees from the normal to the plane of the source. A weighting function was applied to the length of the source to minimize the spread of angles. For the simulation comparing theory and experiment, the simulated source (namely, source 2) consisted of FDTD grid points corresponding to the experimental location of the source relative to the PC which emitted a sinusoidal displacement in both directions of the grid. The vertical and horizontal components of the displacements were weighted such that the spread of angles matched that of the experimental source.

The materials' parameters used were $\rho = 1364$ kg/m^3, $c_t = 1000$ m/s, $c_l = 2230$ m/s for PVC and $\rho = 1.3$ kg/m^3, $c_t = 0$ m/s, and $c_l = 340$ m/s for air. Experimental measurements were obtained from a finite PC consisting of 18 rows and 18 columns of 1-m-long PVC cylinders surrounded with air. The source consisted of the extremity of a Kundt tube with a diameter of 24 mm. We characterized the angular distribution of the experimental source in the absence of the PC by recording amplitude measurements obtained along the direction parallel to the plane of the source at 2 cm and 20 cm away. By defining the width of the beam to be where the amplitude is above 25% of the maximum amplitude at each of the distances from the source, we obtained the angular spread of the output of the source to range from about −45° to 45° from the normal to the plane of the source. Figure 7(a) shows the instantaneous pressure field of the matching FDTD simulated source. It can be seen that the spread of angles is close to that of the experimental measurements.

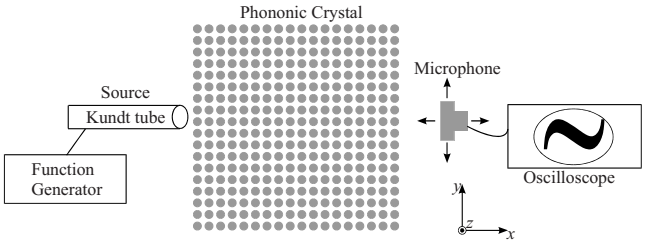

FIG. 1. Schematic diagram of the experimental setup. A source located 1 mm from the center of the input side of the PC consisting of a 24-mm diameter Kundt tube emits at a frequency of 14.1 kHz using a sinusoidal function generator. The phononic crystal consists of an array of 18×18 polyvinylchloride inclusions in an air matrix. Using a receiver and oscilloscope, the image plane is scanned to obtain amplitude measurements. The width of the microphone was 7 mm which is smaller than the wavelength of the acoustic wave in air, thus allowing good spatial resolution of the pressure field.

The source was placed 1 mm away from the center of the PC. The source produced a sinusoidally varying wave, created by a METRIX GX245 function generator. Measurements were obtained using a microphone which scanned across the two-dimensional image plane on the exiting side of the crystal at a height corresponding to that of the source. The width of the microphone was 7 mm, which is smaller than the wavelength of the acoustic wave in air, thus allowing good spatial resolution of the pressure field. Measurements of the pressure field at the exit of the PC were recorded at intervals of 1 mm along the direction parallel to the output surface of the PC and of 5 mm along the direction perpendicular to this surface, using a HAMEQ HM 205–3 oscilloscope. The experimental setup is illustrated in Fig. 1.

III. RESULTS AND DISCUSSION

In order to fully understand the propagation behavior of the waves within the PVC/air phononic crystal, we examine the band structure and corresponding EFSs. Figure 2(a) shows the PWE band structure of the PC for a wave vector describing the principal directions of propagation in the irreducible Brillouin zone (see inset). The straight line represents the dispersion relation in air. Because the air line does not intersect any bands in the irreducible Brillouin zone, we examine the behavior in the extended zone [Fig. 2(b)] along

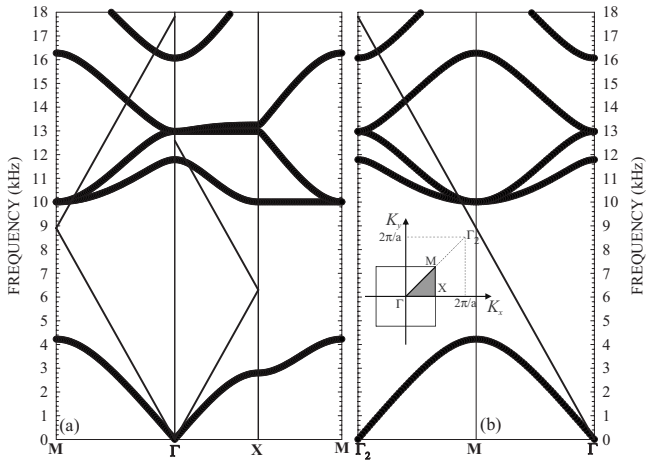

FIG. 2. (a) Band structure along the principal directions of propagation in the irreducible Brillouin zone (see inset). The solid line represents the dispersion curve for air and folds at the edges of the Brillouin zone. (b) Band structure along the ΓM direction in the extended Brillouin zone. The air line intersects the fourth band at a frequency of 14.1 kHz in the extended zone, corresponding to a band exhibiting negative refraction. The components of the wave vector $\vec{K}$ at the Γ, X, and M points are $\frac{2\pi}{a}(0,0)$, $\frac{2\pi}{a}(\frac{1}{2},0)$, and $\frac{2\pi}{a}(\frac{1}{2},\frac{1}{2})$, respectively. The wave vector at the Γ_2 point is $\frac{2\pi}{a}(1,1)$ and is equivalent to that at the Γ point by a translation of a reciprocal-lattice vector.

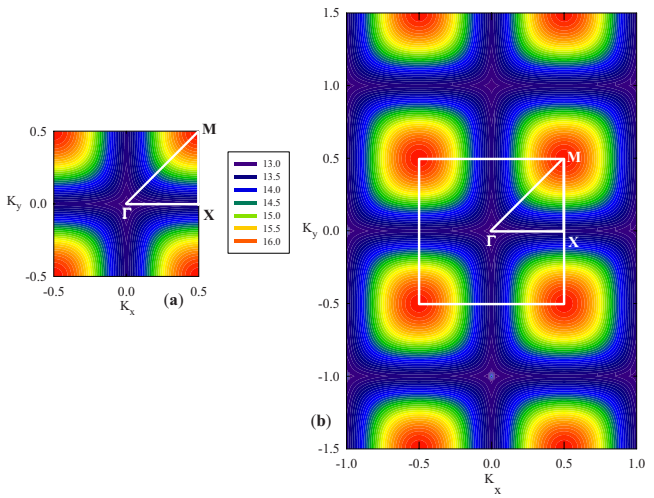

FIG. 3. (Color online) Equifrequency surface corresponding to the fourth band in the first Brillouin zone (a) and in an extended zone scheme (b). The EFS of the PC calculated inside the first Brillouin zone (a) has been repeated by a large number of translations of the reciprocal vectors. One notes that in the extended zone scheme, the EFS are centered on the M point and are of square shape except at their corners. All values on the axes of the EFSs are in units of $\frac{2\pi}{a}$ while values in the color key are in units of kHz.

the Γ M direction. Figure 2(b) shows an intersection of the air line with the fourth band at a frequency of 14.1 kHz ($\lambda = 2.41$ cm in air). Within the irreducible Brillouin zone, the fourth band corresponds to a positive group velocity (i.e., gradient of frequency as a function of wave vector) while in the extended zone scheme, we see that the slope of the band at 14.1 kHz becomes negative. To account for all directions of propagation within the PC, we analyze the corresponding EFS. The EFSs are deduced from the PWE dispersion curves calculated for different directions of propagation of the incident waves. Using a three-dimensional (3D) representation of the dispersion curves [i.e., $\omega(K_x, K_y)$ where ω is the angular frequency and K_x and K_y are the components of the wave vector in the plane perpendicular to the inclusions], the EFSs are obtained from the intersection of the 3D dispersion curves with a horizontal plane, i.e., at fixed frequency. EFSs allow one to determine the wave propagation through the PC from a multitude of different angles by examining the behavior in reciprocal space. Figures 3(a) and 3(b) show the entire EFS in the range of frequencies of the fourth band in the first Brillouin zone and in an extended scheme, respectively. One should note that the shape of the EFS deviates strongly from the circular shape which is required for observing an all angle negative refraction (AANR).[26] At 14.1 kHz the negative refraction may occur in the PVC/air system only within a narrow range of incident angles.

To explore precisely how 14.1 kHz beams, incident at different angles, will propagate through the PC, we use the diagram of Fig. 4. The left part of Fig. 4 shows the first quarter of the EFS for a longitudinal wave propagating in air at 14.1 kHz. The contour of the orange area on the right represents the EFS in the PC for K_x and K_y ranging from 0 to 0.5 (in units of $2\pi/a$) in the first Brillouin zone. The EFS of the PC is also reported for larger values of K_y specifically for $0.5 < K_y < 1$. Note that such values of the component of the wave vector parallel to the interface between the input medium and the PC are equivalent to negative values ranging in the interval $-0.5 < K_y < 0$ by a translation of a reciprocal-lattice vector. The wave vector of the refracted wave inside the PC can be determined by the conservation of the tangential component of the K vector, as well as the direction of propagation through the crystal. Propagation direction within the PC is determined by the gradient at each point on the surface (i.e., the group velocity which points toward the in-

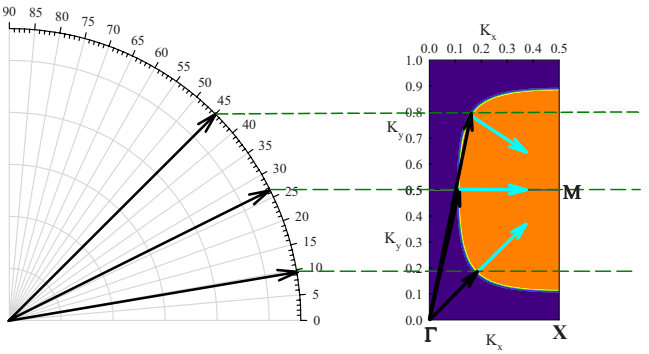

FIG. 4. (Color online) EFS in air and phononic crystal at 14.1 kHz where all angles are measured in degrees. The green dotted lines show the conservation of the component of the wave vector parallel to the interface between air and the input side of the phononic crystal. The light blue arrows represent the group velocity vector inside the phononic crystal. For incidence angles larger than 27°, the wave vector associated with the refracted beam has a negative component along the interface between air and the PC (see text for details).

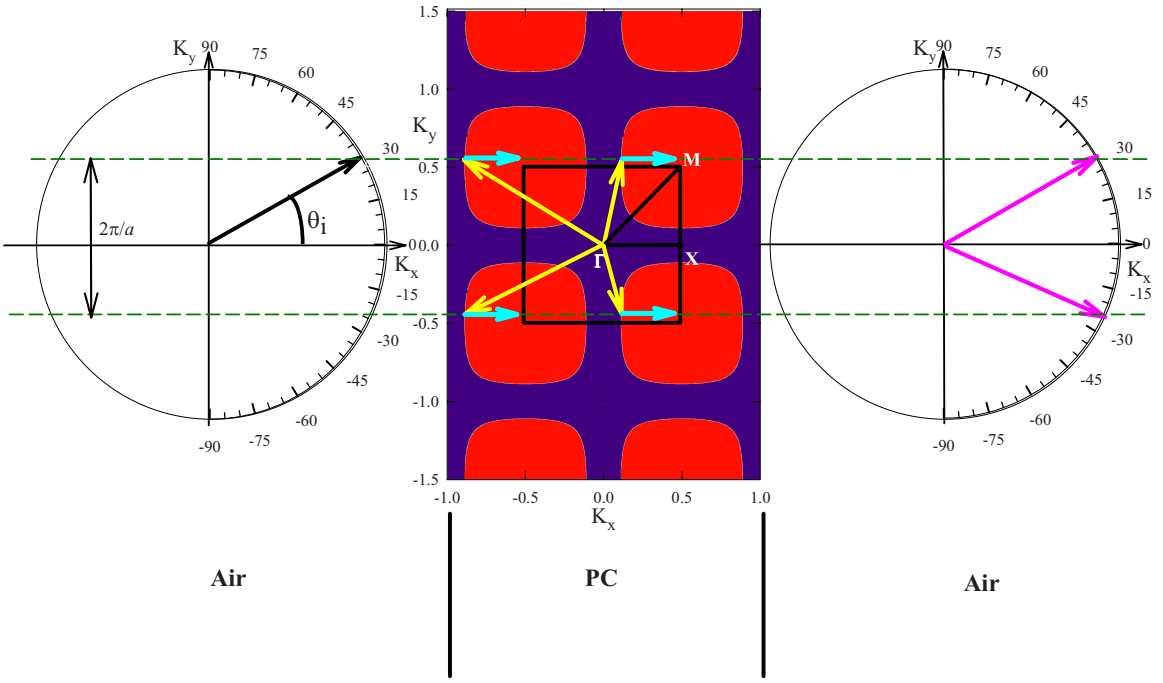

FIG. 5. (Color online) Extended zone scheme of the EFSs of the phononic crystal with corresponding EFSs for air on either side. Blue arrows represent incident and outgoing waves. For an incident beam at an angle of 30° to the horizontal, Bloch waves located on the flat portions of the PCs EFS are excited. Grey arrows represent group velocity vectors whose point toward the increase of frequency (only vectors pointing away from the source are depicted to ensure Poynting's vector is positive). The horizontal green dotted lines indicate phase-matching conditions. Because the EFS of air overlaps multiple EFSs of the crystal, two beams (shown as pink arrows) are able to exit the crystal.

crease of the frequency). From this diagram, one can observe that positive, negative, and zero-angle refraction are possible, depending on the angle of incidence. Three important aspects of the EFS which lead to the different possible types of refraction include the shape of the EFSs and their position with respect to the first Brillouin zone. First, one can see that the EFSs of the PC at 14.1 kHz are nearly square with the exception of the edges which are rounded. Second, the size of the EFSs and the fact that they are not centered on the Γ point of the Brillouin zone allow all excitable Bloch modes to lie within the radius of the EFS of air. Consequently, all signs (positive, negative, and zero) of the group velocity vectors within the crystal can be realized. Incident angles that intersect the flat portion of the EFS correspond to group velocities in the direction perpendicular to the face of the crystal. As a result, the propagating waves undergo zero-angle refraction and are transmitted through the crystal as a collimated beam. Zero-angle refraction occurs for angles of incidence ranging from 15° to 38°. Note that for small angles (lower than 6°), those which do not intersect the EFS, there is no propagation through the crystal. This is in agreement with the observed band gap in the Γ*X* direction of the band structure (see Fig. 1). Positive refraction can occur when the incident angle intersects the lower corner of the EFS. The gradients at these points are directed toward the center of the EFS which result in a positive parallel component K_y of the wave vector. This results in a beam which is positively refracted during propagation through the crystal. If the incident angles are large enough, i.e., closed to 45°, as to intersect the EFS at the upper corner, the incident beam will undergo negative refraction. At these points the gradients of the surface point downward toward the center of the EFS resulting in a negative value of the parallel component of the wave vector (at these points, $0.5 < K_y < 1$, which is equivalent to $-0.5 < K_y < 0$ by a translation of a reciprocal-lattice vector). The incident beam is bent "backward" during propagation through the crystal.

To further our analysis of the propagation of acoustic waves inside the phononic crystal, we examine the wave vector diagram of Fig. 5. The black circles correspond to the contours of the equifrequency surfaces in air at 14.1 kHz and are placed on either side of the extended zone scheme of the EFS in the PC. The EFS of the PC calculated inside the first Brillouin zone [see Fig. 3(a)] has been repeated by a large number of translations of the reciprocal vectors. The equifrequency contours at 14.1 kHz inside the PC are drawn as the contours of the red surfaces. For the sake of clarity, one considers an acoustic wave with an angle of incidence of 30°. All group velocity vectors depicted are those pointing to the right, ensuring that energy is flowing away from the source. Because of the periodicity of the PC, there exist identical group velocity vectors at corresponding points within the entire *K* space of the PC. All wave vectors which lie within the EFS for air satisfy phase-matching conditions and are able to then propagate out of the crystal, leading to multiple outgoing waves.

In the same way, it is found that all angles which are able to propagate (i.e., angles larger than 6°) will undergo beam splitting upon exiting the crystal. This can be attributed to the fact that the incident wave excites Bloch wave vectors

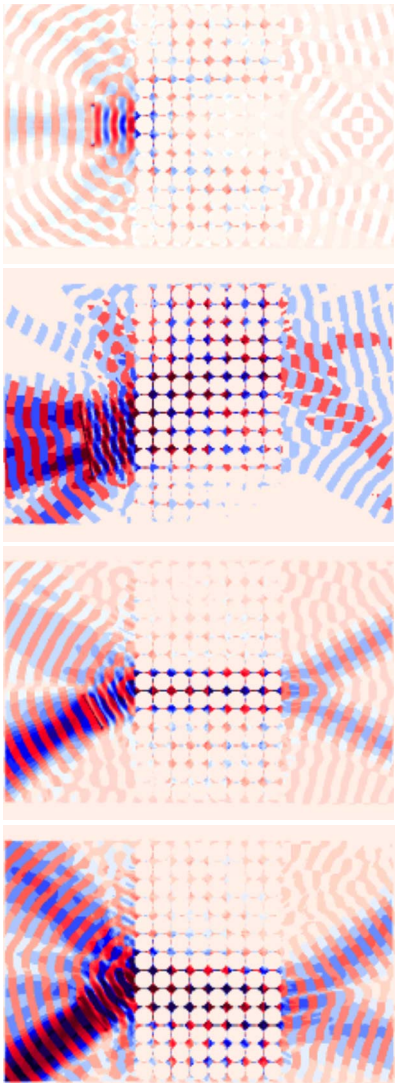

FIG. 6. (Color online) FDTD simulations of the displacement field of a 14.1 kHz plane-wave incident on a PVC/air phononic crystal at different angles using source 1. (a) Plane-wave incident normal to the surface, resulting in little to no transmission. (b) Plane wave incident at 10° to the normal. Beam is positively refracted through the crystal and split upon exit. (c) Plane-wave incident at an angle of 30° to the normal. Beam undergoes zero refraction through the crystal and beam splitting upon exit. (d) Plane-wave incident at 40° to the normal. Beam undergoes negative refraction through the crystal and splitting upon exit.

with a corresponding parallel component within the entire PC. These include both the upward and downward pointing arrows in Fig. 5. The downward pointing arrows are the result of a translation by one reciprocal-lattice vector in the negative direction. As previously mentioned, only the excited Bloch waves which lie within the EFS in air are able to propagate out of the crystal and since for this system, multiple EFSs in the crystal lie within that of air, multiple beams will be seen exiting the crystal for all allowed angles of incidence.

FDTD simulations were used to verify all cases mentioned above. To reduce the computing time, we considered a thinner structure than that used in experiments consisting of 18×10 PVC cylinders surrounded by air. It was confirmed that the results were not significantly modified with a thicker PC slab. A plane-wave source incident on the input side of the PC with different angles of incidence was used. Figure 6(a) shows a plane-wave incident on the input face of the crystal at an angle of 0° to the normal (i.e., perpendicular to the face). The result is that there is little to no transmission of the incident wave through the crystal, as expected from the observed band gap in the ΓX direction of the two-dimensional band structure [Fig. 2(a)]. In Fig. 6(b) a plane wave is incident at an angle of 10° to the normal. At this angle, one can see from the EFS (Fig. 4) that Fourier components of Bloch waves located at the lower corners of the EFS can be excited and a positive refraction at the input side of the PC is obtained. Figure 6(c) shows a plane-wave incident at 30° to the normal. Because this angle intersects the flat portion of the EFS, it is expected that the beam undergo

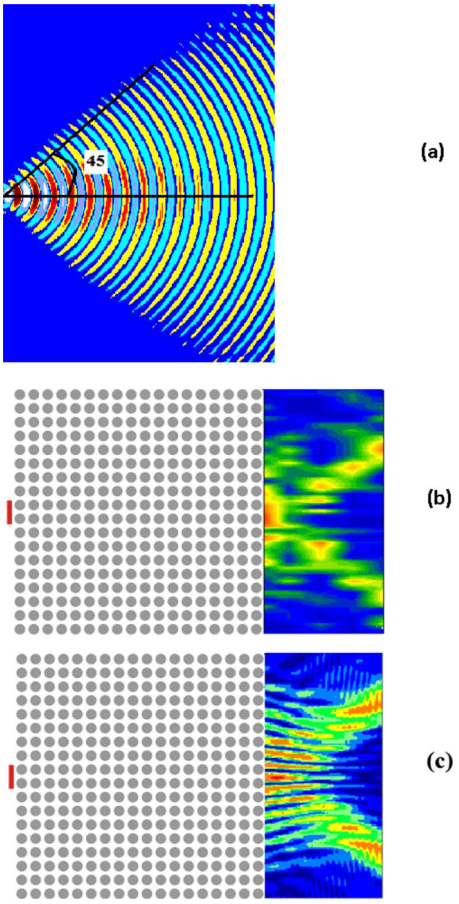

FIG. 7. (Color online) (a) Instantaneous pressure field from an FDTD simulation of source 2 in the absence of the phononic crystal. Plot show a spread of angles of 45° from the normal of the plane of the source, which matches that of the experimental source. (b) Experimental pressure field measured with a 14.1 kHz source located 1 mm from the input side of the PC made of 18×18 PVC cylinders surrounded by air. The map was obtained by scanning a microphone across the image plane and shows an experimental demonstration of beam splitting. (c) FDTD calculation of the average of the absolute value of the pressure over one period at the PC exit. For both plots, the two beams exit the crystal at angles of approximately 25° from the horizontal.

zero refraction through the crystal, which the FDTD simulations are in agreement with. Lastly, we show a beam incident on the crystal at an angle of 40° [Fig. 6(d)]. The EFS shows that at this angle, Fourier components of Bloch waves corresponding to the upper corner will be excited. Because the parallel component of the excited wave vector points opposite to that of the incident beam, negative refraction through the crystal occurs. Finally, as predicted by the EFS (see Fig. 4), in each case depicted in Figs. 6(b)–6(d), the acoustic beam is split into two beams upon exiting the crystal.

Figure 7(b) shows experimental measurements of the amplitude of the pressure field in the image plane of the crystal. Results from an FDTD simulation for an identical system are depicted in Fig. 7(c) which shows the absolute value of the pressure over one cycle. Both figures show beam splitting in which both beams exit the crystal at angles of 25° from the horizontal, providing good agreement between experimental and simulated results. Unlike Figs. 6(a)–6(d) where the source emits at one incident angle, the experimental source in Fig. 7 contains a family of incident angles, all symmetric about the horizontal. The superposition of acoustic waves emitted by this source will exhibit different types of refraction upon entering the phononic crystal including no transmission at low angles of incidence, positive, negative, and zero-angle refraction. Since most of the EFS of the PC is flat with the exception of only a few very small and very large angles, most of the incident angles of the beam excite Bloch waves corresponding to propagation of the wave at an angle close to 0° from the normal (i.e., zero-angle refraction).

The acoustic waves with an angle of incidence of about 27° will exit the PC as two symmetrical beams. This corresponds to an incident wave vector exciting the midpoint of the vertical edge of the EFS of the PC. Waves with incident angles less than or more than 27° will result in asymmetrically split beams. Both sets, each containing two beams, overlap each other and result in the two observed beams exiting the crystal at symmetric angles to the horizontal. The experimental results also confirm beam collimation since the outgoing beams emerge from the crystal over a narrow range of points on the exiting side of the crystal, adjacent to the source. Since most of the EFS of the PC is flat with the exception of only a few very small and very large angles, most of the incident angles of the beam excite Bloch waves corresponding to propagation of the wave at an angle close to 0° from the normal (i.e., zero-angle refraction).

IV. CONCLUSION

Through experimental and theoretical investigations, we demonstrated a system from which positive, negative, and zero-angle refraction can be obtained by varying the angle of the incident beam at a single frequency. Upon exiting the crystal, all allowed angles of incidence underwent beam splitting. Unlike previous demonstrations of these behaviors in phononic crystals, we demonstrated a single periodic system which exhibits all such behaviors. We explained these features in terms of the system's equifrequency surfaces. It was found that a number of characteristics must be present in the EFS's in order to produce the observed behaviors. These included EFSs which were nearly square and whose size and position allowed more than one EFS to overlap with half the EFS of the incident media. This allows all types of wave refraction on the input side of the PC, as well as creates beam splitting upon exit of the PC. Because our system contained all of these features at one frequency, all of the behaviors could be realized by varying only the angle of incidence.

ACKNOWLEDGMENT

J.B. and P.D. would like to thank the IEMN, where some of this work was conducted, for their generosity and hospitality.

[1] E. N. Economou and M. M. Sigalas, Phys. Rev. B **48**, 13434 (1993); J. Acoust. Soc. Am. **95**, 1734 (1994).
[2] M. S. Kushwaha, P. Halevi, L. Dobrzynski, and B. Djafari-Rouhani, Phys. Rev. Lett. **71**, 2022 (1993).
[3] M. S. Kushwaha, B. Djafari-Rouhani, L. Dobrzynski, and J. O. Vasseur, Eur. Phys. J. B **3**, 155 (1998).
[4] M. Kafesaki and E. N. Economou, Phys. Rev. B **60**, 11993 (1999).
[5] I. E. Psarobas, N. Stefanou, and A. Modinos, Phys. Rev. B **62**, 278 (2000).
[6] Z. Liu, C. T. Chan, P. Sheng, A. L. Goertzen, and J. H. Page, Phys. Rev. B **62**, 2446 (2000).
[7] Z. Liu, X. Zhang, Y. Mao, Y. Y. Zhu, Z. Yang, C. T. Chan, and P. Sheng, Science **289**, 1734 (2000).
[8] M. Torres, F. R. Montero de Espinosa, and J. L. Aragón, Phys. Rev. Lett. **86**, 4282 (2001).
[9] J. O. Vasseur, P. A. Deymier, B. Chenni, B. Djafari-Rouhani, L. Dobrzynski, and D. Prevost, Phys. Rev. Lett. **86**, 3012 (2001).
[10] J. H. Page, A. L. Goertzen, S. Yang, Z. Liu, C. T. Chan, and P. Sheng, in *Photonic Crystals and Light Localization in the 21st Century*, NATO Advanced Studies Institute, Series C: Mathematical and Physical Sciences Vol. 563, edited by C. M. Soukoulis (Kluwer, Dordrecht, 2002), p. 59.
[11] S. Yang, J. H. Page, Z. Liu, M. L. Cowan, C. T. Chan, and P. Sheng, Phys. Rev. Lett. **88**, 104301 (2002).
[12] J. H. Page, S. Yang, M. L. Cowan, Z. Liu, C. T. Chan, and P. Sheng, in *Wave Scattering in Complex Media: From Theory to Applications*, NATO Science Series, edited by B. A. van Tiggelen and Sergey Skipetrov (Kluwer Academic Publishers, Amsterdam, 2003), p. 283.
[13] F. Cervera, L. Sanchis, J. V. Sanchez-Perez, R. Martinez-Sala, C. Rubio, F. Meseguer, C. Lopez, D. Caballero, and J. Sanchez-Dehesa, Phys. Rev. Lett. **88**, 023902 (2001); B. C. Gupta and Z. Ye, Phys. Rev. E **67**, 036603 (2003).
[14] N. Garcia, M. Nieto-Vesperinas, E. V. Ponizovskaya, and M. Torres, Phys. Rev. E **67**, 046606 (2003).
[15] S. Yang, J. H. Page, Z. Liu, M. L. Cowan, C. T. Chan, and P. Sheng, Phys. Rev. Lett. **93**, 024301 (2004).

[16] X. Zhang and Z. Liu, Appl. Phys. Lett. **85**, 341 (2004).
[17] J. Witzens, M. Loncar, and A. Scherer, IEEE J. Sel. Top. Quantum Electron. **8**, 1246 (2002).
[18] D. N. Chagrin, S. Enoch, C. M. S. Torres, and G. Tayeb, Opt. Express **11**, 1203 (2003).
[19] P. T. Rakich, M. S. Dahlem, S. Tandon, M. Ibanescu, M. Soljacic, G. S. Petrich, J. D. Joannopoulos, L. A. Kolodziejski, and E. P. Ippen, Nature Mater. **5**, 93 (2006).
[20] D. W. Prather, S. Shi, J. Murakowski, G. J. Schneider, A. Sharkawy, C. Chen, B. Miao, and R. Martin, J. Phys. D **40**, 2635 (2007).
[21] H. Kosaka, T. Kawashima, A. Tomita, M. Notomi, T. Tamamura, T. Sato, and S. Kawakamib, Appl. Phys. Lett. **74**, 1212 (1999).
[22] L. Wu, M. Mazilu, and T. F. Krauss, J. Lightwave Technol. **21**, 561 (2003).
[23] I. Pérez-Arjona, V. J. Sanchez-Morcillo, J. Redondo, V. Espinosa, and K. Staliunas, Phys. Rev. B **75**, 014304 (2007).
[24] V. Espinosa, V. J. Sanchez-Morcillo, K. Staliunas, I. Perez-Arjona, and J. Redondo, Phys. Rev. B **76**, 140302(R) (2007).
[25] J. S. Shi, S. S. Lin, and T. J. Huang, Appl. Phys. Lett. **92**, 111901 (2008).
[26] A. Sukhovich, L. Jing, and J. H. Page, Phys. Rev. B **77**, 014301 (2008).
[27] S. Foteinopoulou and C. M. Soukoulis, Phys. Rev. B **72**, 165112 (2005).
[28] M. S. Wheeler, J. S. Aitchison, and M. Mojahedi, Phys. Rev. B **71**, 155106 (2005).
[29] J. O. Vasseur, P. A. Deymier, M. Beaugeois, Y. Pennec, B. Djafari-Rouhani, and D. Prevost, Z. Kristallogr. **220**, 829 (2005).
[30] D. Garcia-Pablos, M. Sigalas, F. R. Montero de Espinosa, M. Torres, M. Kafesaki, and N. Garcia, Phys. Rev. Lett. **84**, 4349 (2000).
[31] T. Miyashita and C. Inoue, Jpn. J. Appl. Phys., Part 1 **40**, 3488 (2001).
[32] Ph. Lambin, A. Khelif, J. O. Vasseur, L. Dobrzynski, and B. Djafari-Rouhani, Phys. Rev. E **63**, 066605 (2001).
[33] M. Sigalas and N. Garcia, J. Appl. Phys. **87**, 3122 (2000).
[34] G. Mur, IEEE Trans. Electromagn. Compat. **EMC–23**, 377 (1981).